# Organoids Derived from Neoadjuvant FOLFIRINOX Patients Recapitulate Therapy Resistance in Pancreatic Ductal Adenocarcinoma

Elham Aida Farshadi[1], Jiang Chang[2], Bharath Sampadi[3], Michail Doukas[4], Freek Van 't Land[5], Fleur van der Sijde[5], Eveline E. Vietsch[5], Joris Pothof[2], Bas Groot Koerkamp[5], and Casper H.J. van Eijck[5]

## ABSTRACT

**Purpose:** We investigated whether organoids can be generated from resected tumors of patients who received eight cycles of neoadjuvant FOLFIRINOX chemotherapy before surgery, and evaluated the sensitivity/resistance of these surviving cancer cells to cancer therapy.

**Experimental Design:** We generated a library of 10 pancreatic ductal adenocarcinoma (PDAC) organoid lines: five each from treatment-naïve and FOLFIRINOX-treated patients. We first assessed the histologic, genetic, and transcriptional characteristics of the organoids and their matched primary PDAC tissue. Next, the organoids' response to treatment with single agents—5-FU, irinotecan, and oxaliplatin—of the FOLFIRINOX regimen as well as combined regimen was evaluated. Finally, global mRNA-seq analyses were performed to identify FOLFIRINOX resistance pathways.

**Results:** All 10 patient-derived PDAC organoids recapitulate histologic, genetic, and transcriptional characteristics of their primary tumor tissue. Neoadjuvant FOLFIRINOX-treated organoids display resistance to FOLFIRINOX (5/5), irinotecan (5/5), and oxaliplatin (4/5) when compared with treatment-naïve organoids (FOLFIRINOX: 1/5, irinotecan: 2/5, oxaliplatin: 0/5). 5-Fluorouracil treatment responses between naïve and treated organoids were similar. Comparative global transcriptome analysis of treatment-naïve and FOLFIRINOX samples—in both organoids and corresponding matched tumor tissues—uncovered modulated pathways mainly involved in genomic instability, energy metabolism, and innate immune system.

**Conclusions:** Resistance development in neoadjuvant FOLFIRINOX organoids, recapitulating their primary tumor resistance, suggests continuation of FOLFIRINOX therapy as an adjuvant treatment may not be advantageous for these patients. Gene-expression profiles of PDAC organoids identify targetable pathways involved in chemoresistance development upon neoadjuvant FOLFIRINOX treatment, thus opening up combination therapy possibilities.

## Introduction

Pancreatic ductal adenocarcinoma (PDAC) is an exceptionally lethal cancer. Most PDAC patients present with metastatic disease at the time of diagnosis, rendering them ineligible for surgical resection. The average PDAC tumor progression time from resectable to advanced stage is about one year (1). Consequently, most PDAC patients succumb to the disease within a year of diagnosis.

Gemcitabine was the standard treatment for pancreatic patients for more than a decade (2, 3). A more recent chemotherapy regimen, FOLFIRINOX (comprising 5-fluorouracil, irinotecan, and oxaliplatin), improved the overall and progression-free survival when compared with gemcitabine—particularly for patients with advanced disease and in the adjuvant setting (4, 5).

FOLFIRINOX treatment often leads to a stabilization of the disease, or partial response occurs in a minority of the PDAC patients, while others do not respond by showing disease progression during treatment (6). However, even among the responders, most patients develop rapid therapy resistance, resulting in disease progression after treatment. In the clinic, tumor progression following initial regression to chemotherapy presumably originates from the failure of complete eradication of all subclones of cancer cells by current chemotherapy regimens. Such incomplete eradication alters the selection pressure acting on subclones that ultimately favor the outgrowth of resistant clones (7, 8).

Underlying mechanisms of chemoresistance include alterations in several cellular processes, such as metabolic pathways, epithelial–mesenchymal transition (EMT), and angiogenesis resulted in a chemorefractory phenotype in PDAC (9–12). Additionally, stromal tumor components such as cancer-associated fibroblasts and tumor-associated macrophages may promote tumor resistance to chemotherapy (13).

Genomic studies support the notion of homogeneity in disease-initiation events identifying common mutations in four genes: *KRAS, TP53, CDKN2A*, and *SMAD4* (14). Despite this uniformity in aggressiveness and initiating genetic events, PDAC patients display extensive heterogeneity in the response to treatment. This highlights the

[1]Department of Pulmonary Medicine, Erasmus University Medical Center, Rotterdam, the Netherlands. [2]Department of Molecular Genetics, Erasmus MC Cancer Institute, Erasmus University Medical Center, Rotterdam, the Netherlands. [3]Department of Human Genetics, Leiden University Medical Center, Leiden, the Netherlands. [4]Department of Pathology, Erasmus University Medical Center, Rotterdam, the Netherlands. [5]Department of Surgery, Erasmus University Medical Center, Rotterdam, the Netherlands.

**Note:** Supplementary data for this article are available at Clinical Cancer Research Online (http://clincancerres.aacrjournals.org/).

J. Chang and B. Sampadi contributed equally to this article.

**Corresponding Author:** Casper H.J. van Eijck, Department of Surgery, Erasmus University Medical Center, Wytemaweg 80, 3015 CN Rotterdam, the Netherlands. Phone: 31-10-7-033854; E-mail: c.vaneijck@erasmusmc.nl

Clin Cancer Res 2021;27:6602–12

**doi:** 10.1158/1078-0432.CCR-21-1681

## Translational Relevance

Pancreatic ductal adenocarcinoma (PDAC) is an aggressive disease with poor prognosis mainly due to rapid development of therapy resistance. Neoadjuvant FOLFIRINOX in patients with (borderline) resectable pancreatic tumors is increasingly being studied in clinical trials. However, knowledge about FOLFIRINOX resistance mechanisms in a physiologically relevant model is lacking. PDAC organoids derived from resected tumors treated with neoadjuvant FOLFIRINOX could be established and reflect therapy resistance observed in patients, indicating significant resistance to FOLFIRINOX combination therapy as well as oxaliplatin and irinotecan but not to 5-fluoruracil monotherapy. Transcriptome analyses of these organoids revealed genes and pathways that are significantly altered upon FOLFIRINOX treatment. These resistant organoids represent a robust model to investigate drug resistance for personalized therapy. Our study questions application of adjuvant FOLFIRINOX treatment after neoadjuvant treatment, which may be detrimental for patients due to unwanted side effects from oxaliplatin and irinotecan without added treatment value.

prominent role of phenotypic alterations in the development of chemoresistance in pancreatic cancer cells (15).

Understanding the PDAC tumor evolution will be pivotal in delineating mechanisms of chemoresistance and developing strategies to address them. Currently, most studies focused on drug resistance to gemcitabine (16). However, the introduction of the standard of care involving the FOLFIRINOX regimen warrants research into the therapy resistance of PDAC to this novel chemotherapeutic regimen.

In the last decade, comprehensive 3D models of various tumors have been developed recapitulating the biology of primary tumors (17, 18). These patient-derived organoids demonstrated great potential as a research model to predict therapy response in pancreatic cancer and other gastrointestinal cancers (19, 20). However, until now treatment response of residual tumor cells after neoadjuvant FOLFIRINOX has not been investigated in such a 3D patient-derived organoid model. In this study, we generated organoids from resected tumor material of PDAC patients, with or without neoadjuvant treatment before surgery. We investigated the sensitivity/resistance of organoid lines to the individual drugs of the FOLFIRINOX regimen. We demonstrated the utility of organoids from neoadjuvant treated patients as a preclinical model to discover potential targets of therapy failure in PDAC patients.

# Materials and Methods

### Patient samples

Fresh tumor tissues were obtained from PDAC patients operated in Erasmus MC between 2019 and 2020. This study was performed according to the principles of the Declaration of Helsinki, approved by the local medical ethics committee (MEC-2015-085) and all patients provided written informed consent. Patients included in the study completed eight cycles of FOLFIRINOX chemotherapy before resection or were treatment naïve at the time of surgery.

### Establishment of organoids

Tumor tissues were collected and minced into 2–3 $mm^3$ fragments in basic medium [AdDMEM/F12 (Gibco), 1X Hepes (Gibco, #15630), 1X glutamax (Gibco, #35050061), 100 μg/mL piromocin (InvivoGen, #ant-pm-1)]. Tissue fragments were digested in basic media supplemented with 1 mg/mL liberase (TH; Roche, #5401135001), 10 μg/mL DNase I (Sigma, #4263), and 10 μmol/L ROCK inhibitor (Tocris, #1254) for 30 minutes in 37°C.

Digested tissues were filtered and washed with phosphate-buffered saline containing 5% serum to deactivate the enzymes. Pancreatic cells were mounted in matrigel (Corning, #356231) and were cultured in serum-free organoid growth media composed of basic medium supplemented with 1 mmol/L N-acetyl L-cysteine (Sigma, #A9165), 1 mmol/L nicotinamide (Sigma, #N0630), 100 ng/mL mouse recombinant NOGGIN (PeproTech, #250-38), 500 ng/mL recombinant RSPONDIN (PeproTech, #120–38), 25% serum-free WNT conditioned media (21), 50 ng/mL mouse recombinant EGF (Gibco, #PMG8041), 100 ng/mL FGF10 (PeproTech, #100-26), 10 nmol/L gastrin I (Sigma, #G9020), 500 nmol/L A83-01 (Tocris, #2939), and 10 μmol/L Y-27632 dihydrochloride (Tocris, #1254).

### DNA/RNA extraction

We used the AllPrep DNA/RNA mini kit (QIAGEN) to extract both DNA and RNA from organoid samples. Organoids were extracted from matrigel domes using Cell Recovery Solution (Corning, #354253) before adding lysis buffer.

Snap-frozen tumor tissues were used for RNA extraction. Tumor tissues were homogenized [Ultra-Turrax T25 homogenizer (Janke & Kunkel)], and lysed simultaneously. RNA was extracted using the AllPrep DNA/RNA mini kit (QIAGEN).

Paraffin-embedded primary tumor tissue blocks were used for DNA extraction. Five 10-μm-thick FFPE tissue sections were deparaffinized and hematoxylin-stained. Tumor areas were selected and microdissected manually into 5% Chelex 100 Resin (Bio-Rad) and cell lysis solution (Promega), using sterile scalpels. DNA was extracted by proteinase K (Roche) digestion by overnight incubation at 56°C.

### Targeted next-generation sequencing

Extracted DNA was analyzed with next-generation sequencing (NGS) using a panel of 58 cancer-associated genes, including driver genes frequently mutated in PDAC patients (ref. 12; Supplementary Table S1). Library preparation was performed using the Ion AmpliSeq library kit Plus (Thermo Fisher Scientific) with two multiplex PCR reactions (10 ng of DNA per reaction). The Ion AmpliSeq kit protocol was applied to generate amplicon libraries. Libraries were sequenced on the Ion S5XL Semiconductor Sequencer (Thermo Fisher Scientific).

Variants were detected and analyzed by VARIANT CALLER v5.10.0.18 (Thermo Fisher Scientific) and annotated in a local galaxy pipeline (www.galaxyproject.org) using ANNOVAR. Exonic or splice-site variants with at least 5% frequency were selected for analysis. Synonymous point mutations, non-frameshift alterations, and mutations with frequencies greater than 1% in the 1000 Genome database (considered common polymorphisms) were filtered out.

### Drug screening

Organoids were cultured in the same culture condition till confluency. Thereafter, organoids were digested with TrypLE (Gibco 12604-013) for 5 to 10 minutes at 37°C, assisted with mechanical digestion into single cells. 1,000 cells were seeded in 5 μL matrigel domes in a clear-bottomed 96-well plate (3707, Corning). When mature organoids were formed, chemotherapeutic drugs were added. Oxaliplatin (ACCORD, infusion; six doses in the range of $1.2 \times 10^{-6}$ mol/L to $4.02 \times 10^{-5}$ mol/L), 5-FU (ACCORD, infusion; six doses in the range of $3.8 \times 10^{-6}$ mol/L to $1.2 \times 10^{-4}$ mol/L),

SN-38 (TOCRIC #2684; six doses in the range of $5 \times 10^{-10}$ mol/L to $1.6 \times 10^{-8}$ mol/L), gemcitabine (SANDOZ, infusion; six doses in the range, $7 \times 10^{-10}$ mol/L to $2.4 \times 10^{-8}$ mol/L) were tested. FOLFIRINOX regimen was given in five different concentrations by combining the three chemotherapeutic compounds ranging from $6 \times 10^{-7}$ mol/L to $1 \times 10^{-5}$ mol/L for oxaliplatin, $1.9 \times 10^{-6}$ mol/L to $3 \times 10^{-5}$ mol/L for 5-FU, and $1 \times 10^{-10}$ mol/L to $5 \times 10^{-9}$ mol/L for SN-38. Because FOLFIRINOX combination is more potent than monotherapies of its individual components, the range of concentrations was centered around IC25 of its components. FOLFIRINOX drug concentrations represent summed concentrations of its individual components. Cell viability was obtained at baseline day 0 before adding chemotherapeutics and 72 hours after incubation with chemotherapy drugs [CellTiter-Glo 3D (#G9681, Promega); SpectraMax I3 plate reader]. Growth rate values (GR) were obtained by calculation of the baseline median luminescence values of day 0, untreated, and drug-treated day 3 wells (22). Drug concentrations were log transformed, and GR value of each data point was plotted to obtain dose–response curves. $GR_{50}$ values were obtained, and response between two groups was compared using an unpaired *t*-test with Welch correction (GraphPad Prism 9.0).

### Histology and IHC

For processing organoids, full matrigel domes were fixed in 2% paraformaldehyde and 0.2% glutaraldehyde. The matrigel domes were mounted with low melting agar and kept in 4°C before processing for paraffin sectioning. Matrigel-agar blocks were paraffin-embedded, and 4-μm sections were mounted on Superfrost plus slides (Menzel-Gläser), stained with hematoxylin and eosin (H&E; HE600, Ventana, #06917259001) and evaluated by a clinical pathologist.

IHC staining for keratin-19 (CK19) and transcription factor SOX-9 was performed on 4-μm-thick paraffin sections by automated IHC using the Ventana Benchmark ULTRA (Ventana Medical Systems Inc). Sequential 4-μm-thick (FFPE) sections were stained using the Ultraview universal DAB detection kit (#760-700, Ventana).

Antibodies used included 0.11 mg/mL concentration of CK19 mouse monoclonal antibody (clone: A53-B/A2.26; Cell Marque) and 1/750 concentration of SOX-9 anti-goat polyclonal antibody (R&D Systems).

### RNA-seq bioinformatics and data analysis

Poly-A–enriched directional RNA-seq libraries were prepared (Kapa mRNA HyperPrep), and subsequent paired-end read sequencing was performed using the Novaseq 6000 (Illumina; $2 \times 150$ cycles, v1.0 chemistry). After quality control with FastQC, raw sequencing reads were trimmed used Trimmomatic (v 0.36; ref. 23) and aligned to the human reference genome hg38 with TopHat (v 2.0.9). The remaining reads were counted through HTSeq (v 0.6.0; ref. 24). We performed further downstream analyses using Python (NumPy and Pandas packages), R studio (ggplot, DESeq2), Perseus (v 1.5.5.3; ref. 25), Google Sheets, and GraphPad Prism (v 8.3.0). The RNA-seq data set consisting of normalized transcripts per million reads (TPM) for 60,583 genes was $\log_2$ transformed and grouped into 10 different groups, each containing global transcriptomes of two samples (organoid and their respective primary tumor). We filtered the data set to retain genes with one or more read counts (in all 20 samples), resulting in a final matrix consisting of 17,848 genes. Heatmaps display hierarchically clustered genes after preprocessing the data sets with k-means (Euclidean average distance defining the separation between two clusters). To identify differentially expressed genes (DEG), we separated the organoid and primary tumor data and used a combination of two filtering criteria: the first being significantly responding (DESeq2; $P < 0.1$), and the second having a minimum TPM raw (non–log-transformed) value of at least 1 in all samples. Pathway analysis was performed using the Reactome and enrichR databases (reactome.org; $P < 0.05$).

### Data availability

RNA-seq data are available in the GEO repository with the identifier GSE169321.

## Results

### Establishment of a human organoid library of pancreatic cancer after neoadjuvant FOLFIRINOX and treatment-naïve specimens

We have generated a library of 10 organoids from resectable and borderline resectable PDAC patients who received complete eight cycles of neoadjuvant FOLFIRINOX chemotherapy or from patients who were treatment naïve at the time of resection (**Fig. 1A**). The 10 tumor tissues were collected consecutively in time. Clinical characteristics of patients are shown in **Table 1**.

All the organoid lines were cultured with organoid growth media containing essential growth factors as described previously in the literature with some optimization (26, 27). To avoid undefined components in the culture medium, we obtained recombinant RSPONDIN and NOGGIN proteins rather than using conditioned media. Besides, by the use of serum-free WNT conditioned media, we reached the serum content of the medium to zero avoiding the introduction of undefined proteins into the culture. Finally, neoadjuvant FOLFIRINOX organoids tolerated withdrawal of FGF10 growth factor that is essential for the growth of treatment-naïve organoids. Neoadjuvant FOLFIRINOX-treated organoid cultures were successfully established growing at least 10 passages with an efficiency of 83%, whereas the efficiency was 62% for treatment-naïve organoids.

Organoid cultures carried known driver mutations of PDACs evaluated by a panel of cancer-associated genes recapitulating primary tumor origin (**Fig. 1B**; Supplementary Table S1). Our results illustrate that the expected prevalence of driver mutations for PDAC is conserved in our organoid cultures with no significant differences between treatment-naïve and FOLFIRINOX-treated organoid lines (**Fig. 1B** and **C**).

Next, we evaluated whether tumor organoids recapitulate histopathologic characteristics of original tumor tissue. Both neoadjuvant FOLFIRINOX-treated and treatment-naïve pancreatic organoids exhibited mixed morphologies consisting of filled and empty lumen shapes with different degrees of filling (**Fig. 2A**). Although the morphology of the organoids differs between patients, we did not observe any significant morphologic selection associated with FOLFIRINOX treatment (**Fig. 2A**). A high degree of intratumor heterogeneity was observed in primary tumor lesions (**Fig. 2A**, bottom), which is conserved in the corresponding organoid cultures (**Fig. 2A**, top and middle).

Additionally, organoids recapitulate specific features of primary tumor tissue by conserving the expression of epithelial markers (CK19) and expression of pancreatic lineage markers (SOX9). As shown in **Fig. 2B**, expression of CK19 and SOX9 is highly preserved in both treatment-naïve and FOLFIRINOX-treated samples.

### Gene-expression profile is conserved between organoid cultures and paired tumor tissues

To further investigate whether organoids recapitulate their corresponding primary tumor tissue at the molecular level, we performed

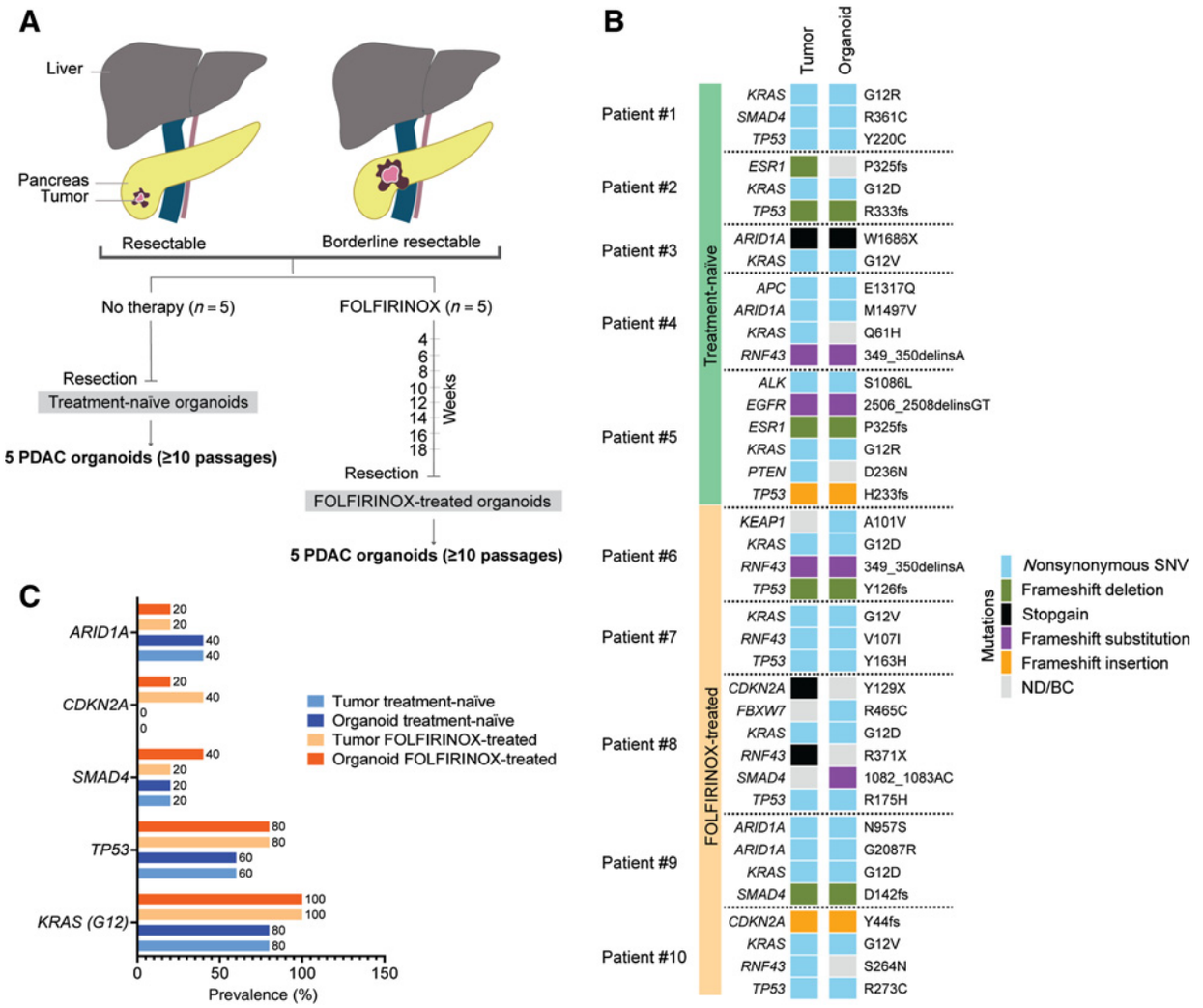


**Figure 1.**

Overview of treatment algorithm, organoid cultures, and their mutational landscape. **A,** Schematic representation of two groups of PDAC patients, and establishment of organoid cultures. Passage 10 corresponds to the success rate for organoid culture. **B,** Targeted sequencing analysis of primary tumors and their corresponding patient-derived organoids. The type of mutations detected in each sample is indicated with colored boxes. If multiple mutations in a gene occurred, only one mutation is shown in this table. ND/BC, not detected/below cutoff. **C,** Bar graph showing prevalence of driver mutations for each group. Blue bars indicate treatment-naïve samples, and orange bars indicate FOLFIRINOX-treated samples. Lighter bars represent tumor samples, and darker bars represent organoids.

mRNA sequencing on 10 tumor organoid cultures (treatment-naïve: O1-O5 and FOLFIRINOX-treated: O6-O10) and 10 corresponding matched tumor tissues (T1-T5 and T6-T10).

Gene-expression profiles were strongly correlated between organoid lines and their corresponding tumor tissues, with a median Pearson correlation coefficient of 0.85 (range, 0.81–0.88; **Fig. 3A**). Principal component analysis showed dispersed and heterogeneous transcription profiles among organoids with a partial separation between treatment-naïve and FOLFIRINOX-treated organoids (**Fig. 3B**). Tumor samples were separated from organoids. Genes that are differentially expressed between paired organoids and tumor tissues are thought to be mainly related to stromal components, or immune cells that are presented in primary tumor lesions but absent in organoids. Further, organoids are exposed to artificial culture conditions to promote cell growth and proliferation. To elucidate these differences, differential gene-expression analysis was performed between cancer organoids and paired tumor tissues. About 2,256/17,848 genes were differentially expressed between organoids and tumor tissues. As shown in the heatmap, most DEGs are highly expressed in primary tumor lesions compared with organoids (**Fig. 3C**). Upregulated genes were enriched for pathways predominantly involved in the tumor microenvironment, immune response, and extracellular matrix (**Fig. 3C**, top right). Whereas downregulated genes were enriched for pathways related to DNA synthesis, mitosis, and proliferation of cancer cells (**Fig. 3C**, bottom right). These DEGs represent only a minority (12%) of the global gene-expression profile that is congruent with a high correlation (**Fig. 3A**) observed between paired tumor and organoid samples. These results indicate that the global gene expression of primary tumor lesions is well conserved in organoid cultures.

**Table 1.** Clinical characteristics of patients.

| | Treatment-naïve | | | | | FFX-treated | | | | |
|---|---|---|---|---|---|---|---|---|---|---|
| **PID** | **T1** | **T2** | **T3** | **T4** | **T5** | **T6** | **T7** | **T8** | **T9** | **T10** |
| Sex/age | F/64 | M/75 | M/78 | F/64 | M/65 | F/51 | M/73 | F/54 | M/68 | F/62 |
| TNM category at diagnosis[a] | cT3N0M0 | cT3N0M0 | cT2N0M0 | cT1N1M0 | cT2N0M0 | cT2N0M0 | cT2N1M0 | cT2N2M0 | cT2N1M0 | cT2N1M0 |
| Stage[a] | IIA | IIA | IB | IIB | IB | IB | IIB | III | IIB | IIB |
| Neoadjuvant therapy | None | None | None | None | None | 8x FFX | 8x FFX | 8x FFX | 8x FFX | 8x FFX |
| Biochemical response[b] | NA | NA | NA | NA | NA | −69 | −278 | 14 | −80 | −186 |
| Radiologic response[c] | NA | NA | NA | NA | NA | SD | SD | SD | PR | SD |
| Histopathologic response[d] | NA | NA | NA | NA | NA | Partial | Partial | Partial | Partial | Partial |
| TNM category at resection[a] | pT3N0 | pT3N2 | pT2N2 | pT1cN0 | pT2N1 | ypT2N0 | ypT2N1 | ypT2N2 | ypT2N2 | ypT2N1 |
| Tumor differentiation | Moderate | Poor | Moderate | Moderate | Moderate | Poor–moderate | Moderate | Moderate | Poor | Poor–moderate |
| Resection margin[e] | R0 | R2 | R0 | R1 | R1 | R0 | R0 | R1 | R1 | R1 |
| Adjuvant therapy | 10x FFX | None | 4x FFX | 5x DC vaccination | 6x FFX | None | None | None | None | None |
| Recurrence | No | Yes | Yes | No | No | Yes | Yes | Yes | Yes | Yes |
| RFS (months) | 24 | 6 | 7 | 17 | 11 | 12 | 12 | 9 | 8 | 11 |
| OS (months) | 24 | 6 | 20 | 17 | 11 | 17 | 15 | 11 | 10 | 13 |

Abbreviations: DC, dendritic cells; FFX, FOLFIRINOX; OS, overall survival; PR, partial response; RFS, recurrence-free survival; SD, stable disease.
[a]According to AJCC 8th edition staging system.
[b]The change in CA19-9 levels between before and after chemotherapy.
[c]According to the RECIST criteria version 1.1.
[d]Partial regression = >5% rest tumor.
[e]According to the definition of the UK Royal College of Pathologists.

### Neoadjuvant FOLFIRINOX-treated organoids show resistance to oxaliplatin and irinotecan monotherapy but not to 5-FU

To evaluate whether surviving cancer cells after neoadjuvant FOLFIRINOX developed resistance to the treatment, we first tested the drug response of five organoid lines (O1–O5) derived from treatment-naïve patients, and five organoid lines (O6–O10) derived from neoadjuvant FOLFIRINOX-treated patients to the individual components of FOLFIRINOX. We quantified cellular growth inhibition metrics of each condition (GR) 72 hours after drug exposure (**Fig. 4** and **A–J**).

Drug response to oxaliplatin indicates four of five FOLFIRINOX-treated organoid lines were markedly resistant when compared with the treatment-naïve organoids (**Fig. 4A**). One of five FOLFIRINOX-treated organoids (O9) showed higher sensitivity to oxaliplatin compared with the rest of FOLFIRINOX-treated samples and clustered with treatment-naïve lines. Computerized tomography evaluation of the primary tumor of this patient (T9) indicated that this was the only patient with a partial response (PR) to neoadjuvant FOLFIRINOX (**Table 1**). The drug-sensitivity results are congruent with the clinical data suggesting the biology of this organoid line is different from the other neoadjuvant patient samples, particularly in the development of chemoresistance to oxaliplatin. We found a significant difference between the $GR_{50}$ values of FOLFIRINOX-treated versus treatment-naïve organoid lines (difference between means ± SE = 15.7 μmol/L ± 5.6) to oxaliplatin monotherapy ($P = 0.03$; **Fig. 4D**).

Drug response to 5-FU varies between different organoid lines (**Fig. 4B**), with no significant difference between FOLFIRINOX-treated and treatment-naïve groups (difference between means ± SE = 8.2 μmol/L ± 6.2; $P = 0.21$; **Fig. 4E**).

Further, we assessed the sensitivity of the organoids to irinotecan therapy (active metabolite SN38; **Fig. 4C** and **F**). Treatment-naïve organoids demonstrate heterogeneous responses to SN38, as three patients (O1, O2, and O4) were sensitive to the drug, while two patients (O3 and O5) were less sensitive to SN38. However, all neoadjuvant FOLFIRINOX-treated organoids were clustering together, showing lower sensitivity to SN38. Our data illustrated a significant difference in sensitivity to SN38 between the neoadjuvant and treatment-naïve (difference between means ± SE = 2.1 nmol/L ± 0.8; $P = 0.04$).

Next, we exposed organoid lines to different concentrations of the FOLFIRINOX combination regimen (obtained by mixing appropriate concentrations of oxalipatin, 5-FU, and SN38) and calculated GR values. All the five FOLFIRINOX-treated organoids displayed a significantly lower sensitivity to the combination treatment when compared with treatment-naïve lines (**Fig. 4G** and **I**; difference between means ± SE = 8.4 μmol/L ± 3.00; $P = 0.02$). Organoid line O3 displayed less sensitivity to FOLFIRINOX, reflecting the clinical resistance of the patient to adjuvant FOLFIRINOX (**Table 1**).

To test whether the chemoresistance is specific to FOLFIRINOX, we exposed all the organoid lines to gemcitabine as a negative control. As it is demonstrated in **Fig. 4H** and **J**, both treatment-naïve and FOLFIRINOX-treated lines respond equally to gemcitabine ($P = 0.90$).

Next, the influence of organoid passage numbers on drug sensitivity was tested by comparing the $GR_{50}$ values obtained from passages three and eight for two organoid lines (O1 and O8) exposed to oxaliplatin and SN-38 monotherapies. We did not find any significant difference between the $GR_{50}$ values obtained from different passages of the same organoids, regardless of the drug used or whether they were treatment-naïve or FOLFIRINOX-treated (Supplementary Fig. S1).

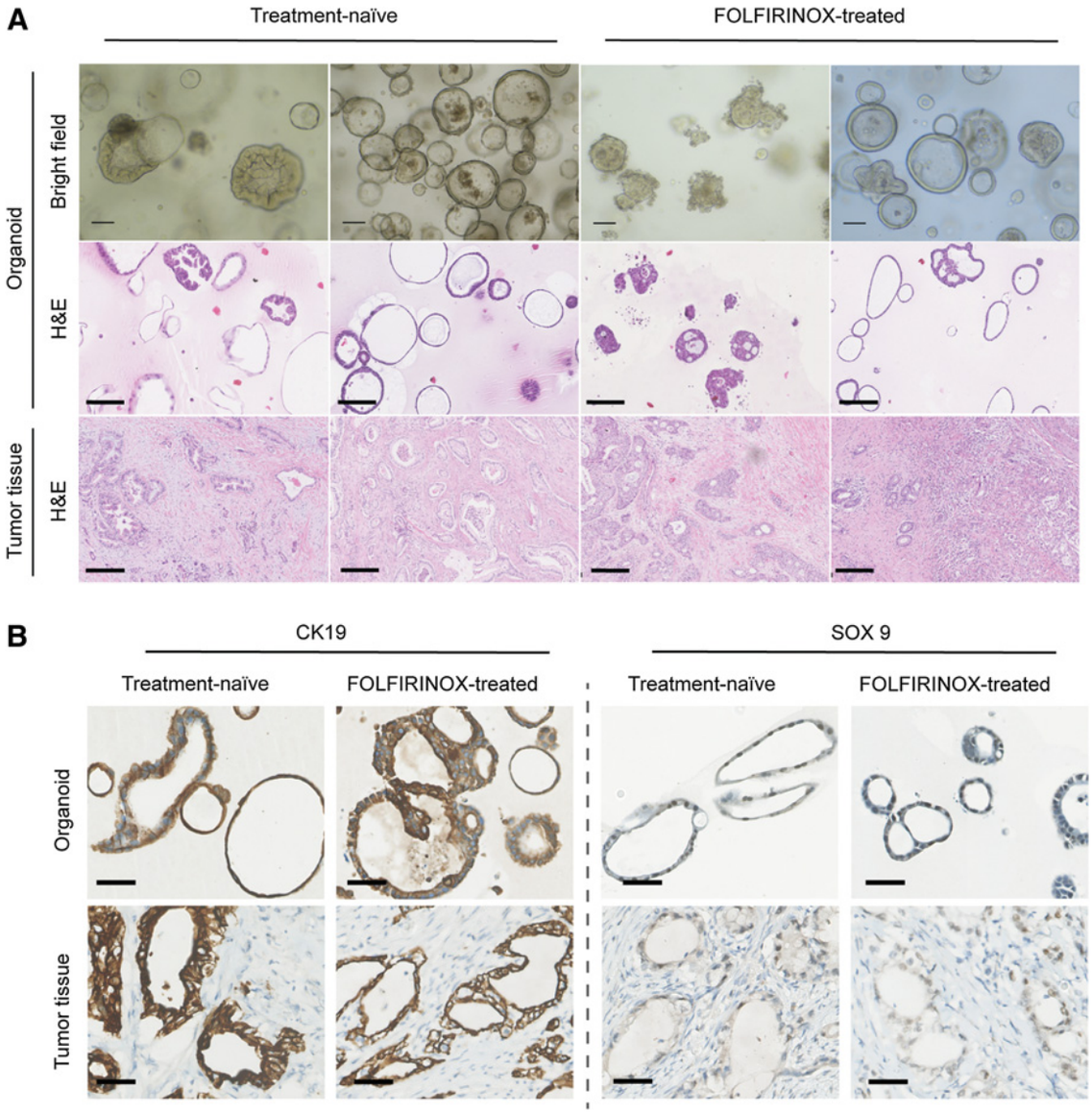


**Figure 2.**

Histologic features of patient-derived PDAC organoids and the corresponding primary tumor tissues. **A,** Representative bright field images of organoid cultures (top), H&E staining (middle) of fixed and sectioned organoids, and H&E staining (bottom) of sectioned parental primary PDAC tissues, from the two patient groups. Scale bars, 100 μm (top row, bright field images) and 250 μmol/L (middle and bottom rows). **B,** Representative images of fixed and sectioned PDAC organoid cultures and parental tumor tissues, immunohistochemically stained for Keratin 19 (CK19), and transcription factor SOX9 protein expression. Images were taken with 40× magnification. Scale bars, 50 μm.

### Global gene-expression analysis identified differentially modulated pathways between treatment-naïve and FOLFIRINOX-treated samples

We performed DEG analysis in organoid cultures and corresponding tumor tissues. We observed 304 DEGs between the treatment-naïve and neoadjuvant FOLFIRINOX groups in primary tumor samples, whereas, in organoid lines, we identified 1,388 DEGs between these two classified groups. Among these, 58 DEGs were common between primary tumors and organoids (**Fig. 5A**). Heatmap visualization displayed the fold-change patterns of these 58 overlapping DEGs in both primary tissues and organoid lines (**Fig. 5B**). Among these genes, 32 were upregulated and 26 were downregulated. Supplementary Fig. S2 illustrates the expression pattern of all individual samples. These overlapping genes provide a set of candidate genes that are independently supported by primary tissues and corresponding organoid cultures.

Pathway analysis of upregulated genes revealed enrichment for pathways mainly involved in genomic instability (genes involved: *TOP2A, EME1*, and *KIF18A*), alternative energy metabolism (genes involved: *SLC2A1, PLA2G4D, MBOAT2*, and *PKM*), and disorders of transmembrane transporters (genes involved: *NET1* and *SLC2A1*; **Fig. 5C**). Conversely, downregulated genes displayed enrichment for

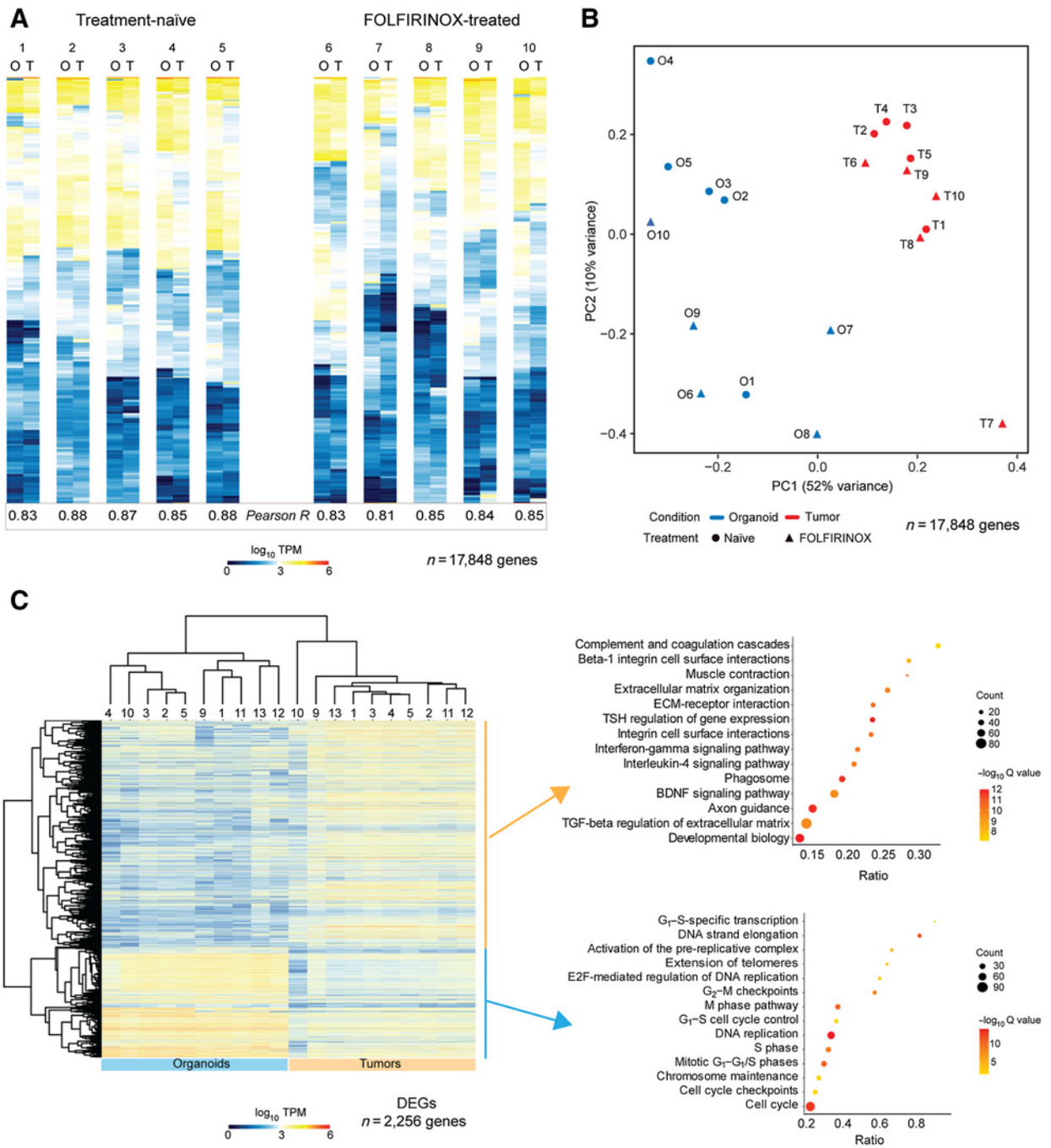


**Figure 3.**

Transcriptome profiles of organoids and matched primary tumors. **A,** Heatmaps of hierarchically clustered genes of 10 organoid lines (O) and their matched primary tumors (T) from two patient groups. Pearson correlation for each organoid–tumor pair is displayed below the heatmap. TPM represents transcripts per million reads. **B,** Principal component analysis (PCA) of the normalized transcript counts. Organoid samples are marked in blue, and tumor samples are marked in red. Treatment-naïve and FOLFIRINOX-treated samples are indicated in closed circles and closed triangles, respectively. **C,** Heatmap of hierarchically clustered DEGs between 10 organoids and 10 tumor samples (left). Right, top 14 KEGG pathways enriched among the upregulated genes (top) and downregulated genes (bottom). Dot size represents the number of genes in each involved pathway. Dot color shows $-\log_{10}$ (*Q* value) in each term enrichment. *X*-axis is ratio of the genes to all the DEGs.

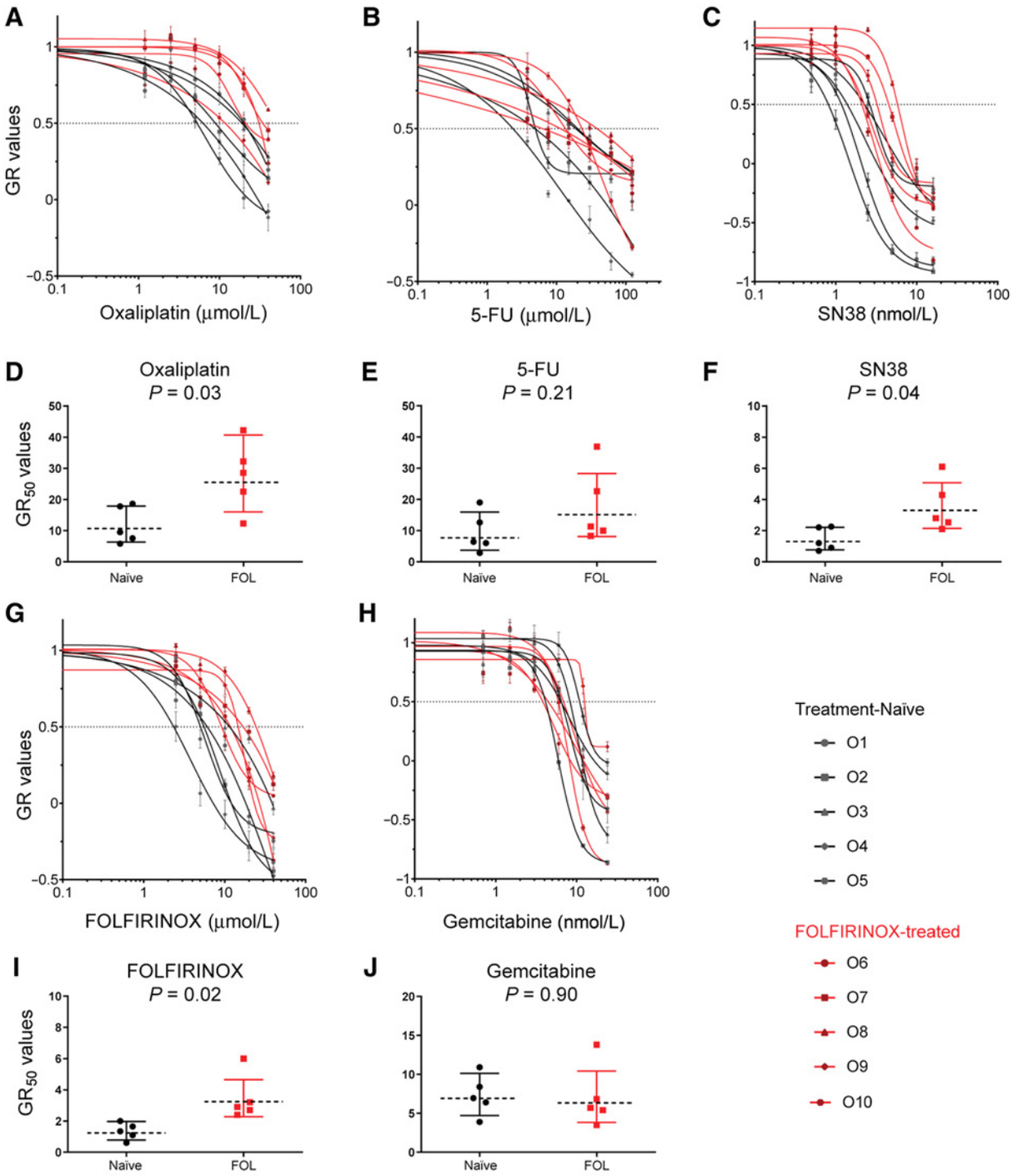


**Figure 4.**

Drug-sensitivity assay of patient-derived organoids. Dose–response curves of 10 patient-derived organoid cultures (passage 7/8) exposed to (**A**) oxaliplatin, (**B**) 5-FU, and (**C**) SN38. Black lines represent treatment-naïve, and red lines represent FOLFIRINOX-treated organoids. *X*-axis shows the logarithmic transformed drug concentrations; *Y*-axis represents the growth rate inhibition values (GR) at 72 hours after drug exposure. Each data point corresponds to the mean of six replicates (two biological experiments with three technical replicates each); error bars, standard error. **D–F,** $GR_{50}$ values for oxaliplatin, 5-FU, and SN38, respectively. Dose–response curves for FOLFIRINOX and gemcitabine are displayed in **G** and **H,** respectively. **I** and **J,** $GR_{50}$ values for FOLFIRINOX and gemcitabine, respectively. Drug responses were compared using an unpaired *t* test with Welch correction.

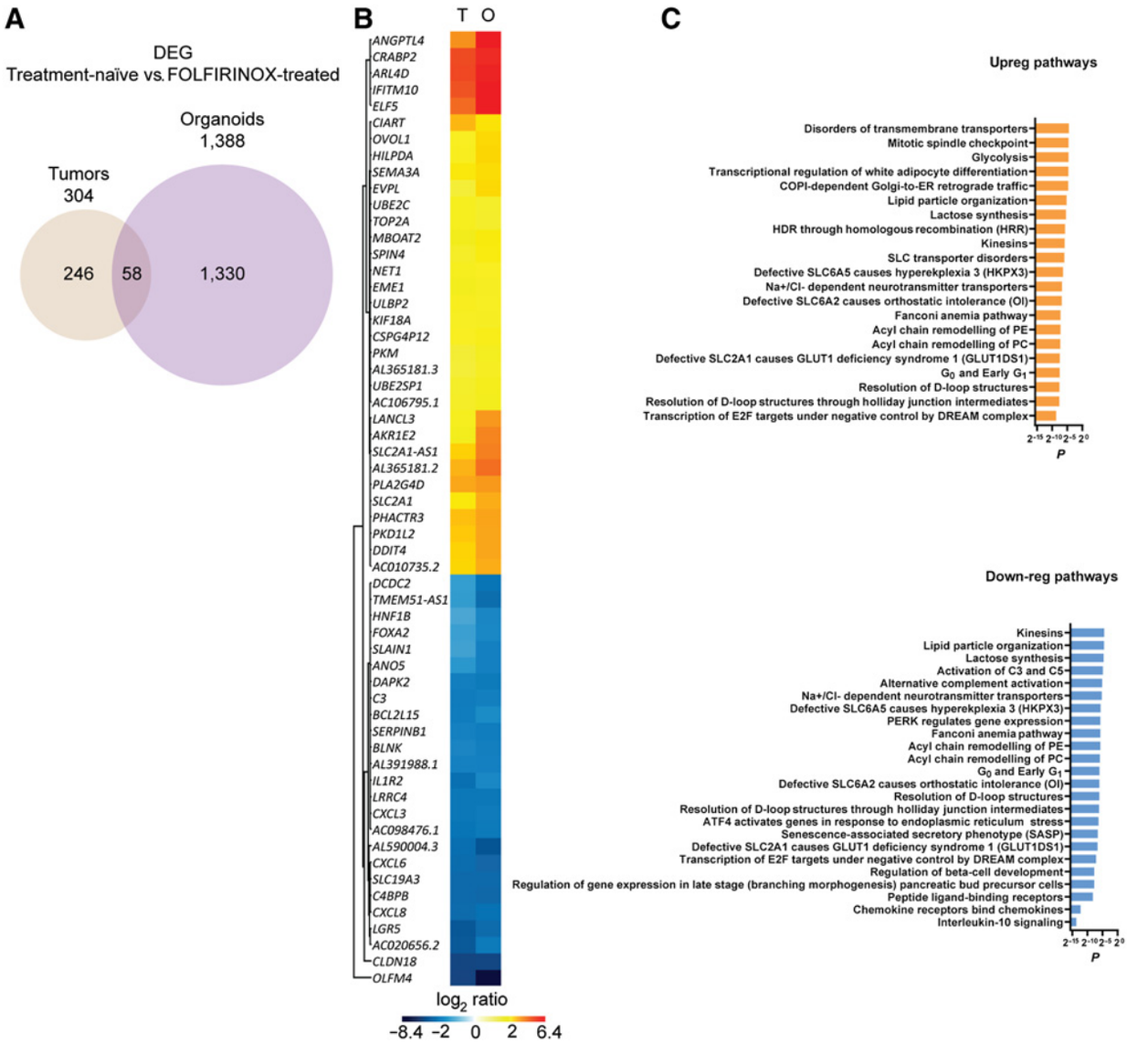


**Figure 5.**

Comparative transcriptome analyses of primary tumor and organoid samples. **A,** Venn diagram of DEGs between treatment-naïve and FOLFIRINOX-treated groups of both primary tumors and organoids. **B,** Heatmap of DEGs in FOLFIRINOX-treated samples versus treatment naïve that overlap in the tumors and organoids. Genes are hierarchically clustered. **C,** Gene ontology (GO) analysis of overlapping upregulated and downregulated genes in the FOLFIRINOX-treated samples. The Reactome database is used to identify significant pathways using a cutoff of $P < 0.05$.

pathways mainly engaged in complement system (genes involved: *C3*and *C4BPB*), immune system (genes involved: *SERPINB1*, BLNK, *OLFM4, CXCL8, CXCL3*, and *IL1R2*), endoplasmic reticulum stress (genes involved: *CXCL8, CXCL3*, and *CXCL6*), and senescence (gene involved: *CXCL8*; **Fig. 5C**).

## Discussion

In this study, we have generated a unique library of organoids from surviving cancer cells obtained from resectable or borderline resectable PDAC tumors from patients who received eight cycles of neoadjuvant FOLFIRINOX treatment as a part of the Dutch pancreatic cancer clinical trial. We also generated organoids from treatment-naïve PDAC lesions that have not been under any selection pressures of chemotherapy. Comprehensive characterization of the organoids confirmed that they recapitulate their matched primary tumor tissues genetically, histologically, and transcriptionally. To our knowledge, no study investigated treatment responses of residual tumor cells after completion of neoadjuvant FOLFIRINOX treatment. FOLFIRINOX-treated organoids showed a resistance profile to oxaliplatin and irinotecan (SN38) monotherapy as well as to FOLFIRINOX combination therapy compared with treatment-naïve organoid lines, suggesting a clonal sweep of resistant clones under the selection pressure of these drugs (7). However, we did not

observe any particular resistance profile to 5-FU monotherapy. Furthermore, organoids in both cohorts displayed equal sensitivity to gemcitabine, suggesting that the chemoresistance observed toward FOLFIRINOX is specific to this therapy. These data suggest that the chemotherapy regimen for PDAC patients needs to be determined at the individual level, because adjuvant therapy with oxaliplatin and irinotecan may not be beneficial for all patients after neoadjuvant FOLFIRINOX therapy.

The organoid line O9 derived from tumor material of a patient with PR to neoadjuvant FOLFIRINOX was the only exception. This particular organoid line (O9) was sensitive to oxaliplatin *in vitro* but resistant to irinotecan and FOLFIRINOX combination therapy. The oxaliplatin sensitivity of this organoid line recapitulates the better overall clinical response of patient to FOLFIRINOX. Congruently, Tiriac and colleagues (13) generated treatment-naïve organoids and showed that the patient's clinical response to FOLFIRINOX was strongly correlated to the oxaliplatin monotherapy response *in vitro*.

The clinical drug response of the three of five treatment-naïve patients who received adjuvant FOLFIRINOX therapy mirrored the *in vitro* drug-sensitivity response of their corresponding organoid models for FOLFIRINOX regimen, indicating that our organoid model may predict clinical drug sensitivity of the patient. However, this result must be verified in a bigger cohort of patient materials. PDAC patients (belonging to the neoadjuvant FOLFIRINOX cohort) were initially all responsive; therefore, they could complete eight cycles of chemotherapy and underwent tumor resection. However, the corresponding neoadjuvant FOLFIRINOX-treated organoids generated from residual tumor cells that escaped the treatment do not represent the initial clinical response of the patient.

Tumor-extrinsic factors (such as cancer-associated fibroblasts and immune cells) that are absent in the organoid cultures may promote therapy resistance in patients (13). Therefore, the impact of tumor microenvironment in the development of chemoresistance of patients should be investigated further in a more complex model.

We evaluated the mutational pattern of organoids by performing targeted NGS on a panel of cancer-associated genes (Supplementary Table S1), including the five known somatic driver gene mutations for pancreatic patients: *KRAS*, *P53*, *CDKN2A*, *SMAD4*, and *ARID1A* (9). The prevalence of driver mutations for PDAC in the primary tumors is conserved in our organoid cultures with no significant differences in the ratio of driver gene mutations in treated versus treatment-naïve organoids. Homogeneity in the mutational landscape of FOLFIRINOX-treated and treatment-naïve organoids suggests that resistant clones might originate from heterogeneity in nongenetic factors, such as different levels of receptor activity, differentiation state, and metabolism (8). Consistently, the diversity in the transcriptome profiles of these organoids and the partial segregation of samples based on the FOLFIRINOX treatment regime—both in primary tumor tissues and organoid samples—suggest gene expression could be related to the heterogeneity in treatment response.

We identified 58 core DEGs (treatment-naïve vs. FOLFIRINOX-treated) that overlapped between primary tumor lesions and their corresponding organoid cultures. Some of the pathways associated with alteration in these candidate genes are involved in crucial chemoresistance mechanisms and tumorigenesis of cancer cells, as reported by several studies. For instance, overexpression of *PKM* and *SLC2A* genes in the FOLFIRINOX patient samples is associated with altered metabolism leading to the survival of the cancer cells under stress conditions, which eventually confers drug resistance (28, 29). Furthermore, overexpression of the *KIF18A* gene is strongly associated with the proliferation and survival of cancer cells (30). Conversely, pathways engaged in cellular senescence (*CXCL8*) and innate immunity (*C3, CXCL8*) were downregulated in the FOLFIRINOX-treated group. Targeted therapies inducing senescence in PDAC cells lead to increased vascular remodeling in the tumor microenvironment of PDAC, rendering cells susceptible to gemcitabine-based chemotherapy and immunotherapy (12). Finally, downregulation in innate immunity is considered as a prognostic factor mediating the survival and metastasis of cancer cells (31).

In conclusion, our neoadjuvant FOLFIRINOX organoids provide an attractive model to predict responsiveness to therapeutic regimens *in vivo* and investigate therapy failure in pancreatic cancer patients. Our findings warrant more in-depth investigations to identify crucial elements of therapy resistance of each patient. These investigations might ultimately lead us to design and optimize a personalized strategy for combined chemotherapy regimens following neoadjuvant FOLFIRINOX therapy.

## Authors' Disclosures

No disclosures were reported.

## Authors' Contributions

**E.A. Farshadi:** Conceptualization, data curation, software, formal analysis, supervision, validation, investigation, visualization, methodology, writing–original draft, project administration, writing–review and editing; the project, designed and performed all experiments, analyzed data sets, and wrote the manuscript. **J. Chang:** Software and formal analysis; analyzed RNA-seq data and provided related figures. **B. Sampadi:** Software, formal analysis, visualization, writing–review and editing; contributed with analyzing the RNA-seq data, providing related figures and provided inputs for writing the manuscript. **M. Doukas:** Writing–review and editing; contributed with all the pathologic assessments and supported collection of patients materials. **F. Van 't Land:** Data curation; provided patients' clinical information and followed up patients. **F. van der Sijde:** Data curation, writing–review and editing; contributed with technical assistance during the study. **E.E. Vietsch:** Data curation, writing–review and editing; contributed with technical assistance during the study. **J. Pothof:** Supervised Jiang Chang. **B.G. Koerkamp:** Resources, writing–review and editing; supported collection of patients materials and reviewed the manuscript. **C.H.J. van Eijck:** Conceptualization, resources, supervision, funding acquisition, writing–review and editing; contributed with supervision, study implementation, writing and reviewing the manuscript, and collection of patient materials.

## Acknowledgments

We would like to thank the members of Prof. Riccardo Fodde laboratory for technical assistance. This study was funded by Stichting Overleven met Alvleesklierkanker.

The costs of publication of this article were defrayed in part by the payment of page charges. This article must therefore be hereby marked *advertisement* in accordance with 18 U.S.C. Section 1734 solely to indicate this fact.

Received May 11, 2021; revised August 26, 2021; accepted September 21, 2021; published first September 27, 2021.

## References

1. Yu J, Blackford AL, dal Molin M, Wolfgang CL, Goggins M. Time to progression of pancreatic ductal adenocarcinoma from low-to-high tumour stages. Gut 2015;64:1783.
2. Oettle H, Neuhaus P, Hochhaus A, Hartmann JT, Gellert K, Ridwelski K, et al. Adjuvant chemotherapy with gemcitabine and long-term outcomes among

patients with resected pancreatic cancer: the CONKO-001 randomized trial. JAMA 2013;310:1473.
3. Khorana AA, Mangu PB, Berlin J, Engebretson A, Hong TS, Maitra A, et al. Potentially curable pancreatic cancer: American Society of Clinical Oncology Clinical Practice Guideline. JCO 2016;34:2541–56.
4. Conroy T, Desseigne F, Ychou M, Bouché O, Guimbaud R, Bécouarn Y, et al. FOLFIRINOX versus gemcitabine for metastatic pancreatic cancer. N Engl J Med 2011;364:1817–25.
5. Conroy T, Hammel P, Hebbar M, Ben Abdelghani M, Wei AC, Raoul J-L, et al. FOLFIRINOX or gemcitabine as adjuvant therapy for pancreatic cancer. N Engl J Med 2018;379:2395–406.
6. Perri G, Prakash L, Malleo G, Caravati A, Varadhachary GR, Fogelman D, et al. The sequential radiographic effects of preoperative chemotherapy and (chemo) radiation on tumor anatomy in patients with localized pancreatic cancer. Ann Surg Oncol 2020;27:3939–47.
7. Vasan N, Baselga J, Hyman DM. A view on drug resistance in cancer. Nature 2019;575:299–309.
8. Pribluda A, de la Cruz CC, EL J. Intratumoral heterogeneity: from diversity comes resistance. Clin Cancer Res 2015;21:2916–23.
9. Viale A, Pettazzoni P, Lyssiotis CA, Ying H, Sánchez N, Marchesini M, et al. Oncogene ablation-resistant pancreatic cancer cells depend on mitochondrial function. Nature 2014;514:628–32.
10. Grasso C, Jansen G, Giovannetti E. Drug resistance in pancreatic cancer: Impact of altered energy metabolism. Crit Rev Oncol Hematol 2017;114:139–52.
11. Zheng X, Carstens JL, Kim J, Scheible M, Kaye J, Sugimoto H, et al. Epithelial-to-mesenchymal transition is dispensable for metastasis but induces chemoresistance in pancreatic cancer. Nature 2015;527:525–30.
12. Ruscetti M, Morris JP, Mezzadra R, Russell J, Leibold J, Romesser PB, et al. Senescence-induced vascular remodeling creates therapeutic vulnerabilities in pancreas cancer. Cell 2020;181:424–41.
13. Zitvogel L, Apetoh L, Ghiringhelli F, Kroemer G. Immunological aspects of cancer chemotherapy. Nat Rev Immunol 2008;8:59–73.
14. Waddell N, Pajic M, Patch A-M, Chang DK, Kassahn KS, Bailey P, et al. Whole genomes redefine the mutational landscape of pancreatic cancer. Nature 2015; 518:495–501.
15. Swayden M, Iovanna J, Soubeyran P. Pancreatic cancer chemo-resistance is driven by tumor phenotype rather than tumor genotype. Heliyon 2018;4:e01055.
16. Adamska A, Elaskalani O, Emmanouilidi A, Kim M, Abdol Razak NB, Metharom P, et al. Molecular and cellular mechanisms of chemoresistance in pancreatic cancer. Adv Biol Regul 2018;68:77–87.
17. Tuveson D, Clevers H. Cancer modeling meets human organoid technology. Science 2019;364:952–5.
18. Fujii M, Sato T. Somatic cell-derived organoids as prototypes of human epithelial tissues and diseases. Nat Mater 2021;20:156–69.
19. Tiriac H, Belleau P, Engle DD, Plenker D, Deschênes A, Somerville TDD, et al. Organoid profiling identifies common responders to chemotherapy in pancreatic cancer. Cancer Discov 2018;8:1112–29.
20. Vlachogiannis G, Hedayat S, Vatsiou A, Jamin Y, Fernández-Mateos J, Khan K, et al. Patient-derived organoids model treatment response of metastatic gastrointestinal cancers. Science 2018;359:920–6.
21. Mihara E, Hirai H, Yamamoto H, Tamura-Kawakami K, Matano M, Kikuchi A, et al. Active and water-soluble form of lipidated Wnt protein is maintained by a serum glycoprotein afamin/a-albumin. eLife 2016;19:e11621.
22. Hafner M, Niepel M, Sorger PK. Alternative drug sensitivity metrics improve preclinical cancer pharmacogenomics. Nat Biotechnol 2017;35:500–2.
23. Bolger AM, Lohse M, Usadel B. Trimmomatic: a flexible trimmer for Illumina sequence data. Bioinformatics 2014;30:2114–20.
24. Anders S, Pyl PT, Huber W. HTSeq–a Python framework to work with high-throughput sequencing data. Bioinformatics 2015;31:166–9.
25. Tyanova S, Temu T, Sinitcyn P, Carlson A, Hein MY, Geiger T, et al. The Perseus computational platform for comprehensive analysis of (prote)omics data. Nat Methods 2016;13:731–40.
26. Boj SF, Hwang C-I, Baker LA, Chio IIC, Engle DD, Corbo V, et al. Organoid models of human and mouse ductal pancreatic cancer. Cell 2015;160: 324–38.
27. Seino T, Kawasaki S, Shimokawa M, Tamagawa H, Toshimitsu K, Fujii M, et al. Human pancreatic tumor organoids reveal loss of stem cell niche factor dependence during disease progression. Cell Stem Cell 2018;22:454–67.
28. Taniguchi K, Sakai M, Sugito N, Kuranaga Y, Kumazaki M, Shinohara H, et al. PKM1 is involved in resistance to anti-cancer drugsBiochemical and Biophys Res Commun 2016;473:174–80.
29. Song K, Li M, Xu X-J, Xuan L, Huang G-N, Song X-L, et al. HIF-1α and GLUT1 gene expression is associated with chemoresistance of acute myeloid leukemia. Asian Pac J Cancer Prev 2014;15:1823–9.
30. Marquis C, Fonseca CL, Queen KA, Wood L, Vandal SE, Malaby HLH, et al. Chromosomally unstable tumor cells specifically require KIF18A for proliferation. Nat Commun 2021;12:1213.
31. Reis ES, Mastellos DC, Ricklin D, Mantovani A, Lambris JD. Complement in cancer: untangling an intricate relationship. Nat Rev Immunol 2018;18: 5–18.